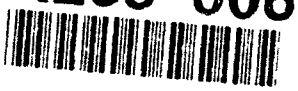

TM No. 921240

Preliminary Results On Backscattering Strength From A Wind Generated Bubbly Ocean Surface

Edward Y. T. Kuo

Naval Undersea Warfare Center, New London Detachment
New London, Connecticut 06320

November 25, 1992

REPORT DOCUMENTATION PAGE

Form Approved
OMB No. 0704-0188

1. AGENCY USE ONLY (Leave blank)	2. REPORT DATE	3. REPORT TYPE AND DATES COVERED
	25 November 1992	TECHNICAL MEMORANDUM

4. TITLE AND SUBTITLE
Preliminary Results on Backscattering Strength from a Wind Generated Bubbly Ocean Surface

5. FUNDING NUMBERS

6. AUTHOR(S)
Edward Y.T. Kuo

7. PERFORMING ORGANIZATION NAME(S) AND ADDRESS(ES)
Naval Undersea Warfare Center
New London Detachment
New London, CT. 06320

8. PERFORMING ORGANIZATION REPORT NUMBER
TM 921240

9. SPONSORING/MONITORING AGENCY NAME(S) AND ADDRESS(ES)

10. SPONSORING/MONITORING AGENCY REPORT NUMBER

11. SUPPLEMENTARY NOTES

12a. DISTRIBUTION/AVAILABILITY STATEMENT
Approved for public release; distribution is unlimited

12b. DISTRIBUTION CODE

13. ABSTRACT (Maximum 200 words)

This report summarizes a preliminary result contained in an upcoming paper [1] documenting continuing research effort in bubbly ocean surface scattering. As such, details will be referred to that paper. This report is written for a timely comparison with different sets of experimental data and is hoped to shed some light on a possible reason why there were apparent differences among experimental data sets.

Since the ONR Special Research Program (SRP) has publicized the importance of bubbly ocean surface effect on acoustic scattering, many papers dealing with the subject have appeared. The model described in this paper is based in part on a NATO presentation[2] delivered in May 1992.

14. SUBJECT TERMS	15. NUMBER OF PAGES
Acoustic Scattering Strength Bubbly Ocean Surface	31
	16. PRICE CODE

17. SECURITY CLASSIFICATION OF REPORT	18. SECURITY CLASSIFICATION OF THIS PAGE	19. SECURITY CLASSIFICATION OF ABSTRACT	20. LIMITATION OF ABSTRACT
Unclassified	Unclassified	Unclassified	

Abstract

This report summarizes a preliminary result contained in an upcoming paper[1] documenting continuing research effort in bubbly ocean surface scattering. As such, details will be referred to that paper. This report is written for a timely comparison with different sets of experimental data and is hoped to shed some light on a possible reason why there were apparent differences among experimental data sets.

Since the ONR Special Research Program (SRP) has publicized the importance of bubbly ocean surface effect on acoustic scattering, many papers dealing with the subject have appeared. The model described in this paper is based in part on a NATO presentation[2] delivered in May 1992.

Administrative Information

This documentation was supported by (1) Multi-Static Sonar program project number D20027, principal investigator R. Christian, program manager C. Mason, sponsoring activity NAVSEA PEO USW ASTO, program manager D. Spires and (2) Critical Sea Test program project number C60807, principal investigator J. Chester, program manager R. Malone. sponsoring activity SPAWAR PMW 182-5, program manager C. Bohman.

1. Introduction to the Model

Consider an incident plane wave velocity potential ϕ_i = $\exp[i(\underline{k}_i \cdot \underline{x} - \omega t)]$ entering the wind generated bubbly surface layer from below (see Fig. 1), where $\underline{k}_i = k(\alpha,\beta,-\gamma)$, k = incident acoustic wave number, $(\alpha,\beta,-\gamma)$ = incident wave direction cosines, ω = circular acoustic frequency, t = time, $\underline{x} = (\underline{x}_{2D},z) = (x,y,z)$ = 3D position vector, $\underline{x}_{2D} = (x,y)$ = horizontal position vector, and z = mean depth. The objective is to estimate the total field of reflected waves coming down from the bubbly layer. Due to a rough ocean boundary and fluctuating sound velocity of the layer medium, there will be both surface and volumetric scattering. Within the single scattering theory, there are two chains of alternating volume and surface scattering events.

The first chain starts from the volumetrical scattering of the incident wave. Then the up-going volumetrically scattered waves will be surface scattered, and volumetrically scattered again. As described in reference 3, single surface scattering can be symbolically characterized by a multiplication factor of $(1+dA+dAdA^*)$ where dA is a Fourier Stieljes component of the surface roughness η, i.e., $\eta(\underline{x}_{2D}) = \int \exp[-ik_{2D} \cdot \underline{x}_{2D}]dA(\underline{k}_{2d})$. The single volumetric scattering can be shown to be symbolically characterized by a multiplication factor $d\Gamma$, which is a Fourier Stieljes component of $(\delta c/c_0)$, the fractional acoustic velocity fluctuation i.e. $2k^2(\delta c/c_0) = \int \exp(-i\underline{k} \cdot \underline{x})d\Gamma(\underline{k}) = \int \exp(-i\underline{k} \cdot \underline{x})\Gamma(\underline{k})d\underline{k}$. Because both dA and $d\Gamma$ are considered small perturbation parameters, the scattered field generated by the

alternating repeated scattering events will eventually become negligible - beyond second order in dA and dΓ.

The second chain starts from a rough surface scattered wave ϕ_s. According to the single volumetric scattering described by Batchelor[4], the incident wave ϕ_i will penetrate the bubbly layer approximately unchanged despite the ongoing volumetric scattering described above. The scattered waves ϕ_s will be volumetrically scattered and followed by the similar alternating scattering processes as in the first chain until the scattered waves become negligible. The total reflected and scattered field is the combination of all the down-going waves generated by every surface and volumetric scattering events or processes described above. The detail of obtaining the total reflected and scattered field can be found in reference 1. In this report, major steps taken in reaching a solution will be summarized.

For each volumetric scattering, the first Born's approximation as presented by Batchelor[4] is assumed appropriate - the single volumetric scattering approximation. Previous investigators McDonald[5] and Henyey[6] utilized the same approximation. In addition, they also utilized, as Batchelor[4] did, the far-field approximation for an individual plume. Approach here, however, do not identify individual plumes. A continuous layer (without an abrupt mean impedance discontinuity) of an infinite horizontal extent is assumed to exhibit random sound velocity fluctuations induced by those plumes which appear randomly in space and time. Volumetrically scattered waves are divided into two groups. The first group propagates away from

the sea surface and contributes directly to the reflected field. The second group propagates toward rough sea surface and surface scattered. Since volumetric scatterers are near ocean surface, these up-going volumetrically scattered waves should be in near-field forms.

For each sea surface scattering, the reflected/scattered field is obtained by applying a perturbation method[3] to a pressure release boundary condition. Most of the reflected energy contributes directly to the reflected field below the bubbly sea surface layer. A small part will be volumetrically scattered as described above.

The total reflected field $\phi_r(\underline{x}_{2D}, z, t)$ consists of all above down-going (away from ocean surface) waves. To the second order in $d\Gamma$ and dA, there are a total of nine component waves. These component waves are re-grouped according to the perturbation order. It can be shown that four of these component waves without the surface roughness combine into the basic results before far-field approximation utilized by McDonald[5] and Henyey[6]. At this stage, the total reflected field is expressed in terms of random variables $d\Gamma$ and dA as a result of turbulent wind action. Therefore, the total reflected field takes different values from one realization to another and only statistical averages are relevant. An appropriate statistical analysis is described in the following section.

2. Statistical Analysis and the Backscattering Strength Predictive Model

Before applying an appropriate statistical analysis, relationships between $(\delta c/c_0)$ and other measurable physical parameters should be investigated. This approach will make it possible not only to evaluate consistencies of different physical parameter measurements, but also to enable a use of particular physical parameters that are easier to measure for scattering strength predictions. As shown in reference 1, these relationships can be summarized into one general form:

$$(\delta c/c_0) = -F_\chi \exp(-\beta z)\chi(\underline{x}_{2D}) \qquad (2\text{-}1)$$

... in which exponential depth decay with decay constant β is assumed. χ represents one of random surface characteristics in a horizontal space $\underline{x}_{2D}$ such as fractional acoustic velocity fluctuation $(\delta c/c_0)_s$, number of bubbles per unit volume N_0, roughness element height η_k, fraction of sea surface covered by white caps W, and acoustic scattering cross-section per unit volume M_{v0}. F_χ is the corresponding coefficient for each χ selected. Expressions of these coefficients are given in the following. The minus sign in equation (2-1) came from an expression relating $(\delta c/c_0)$ to N at a depth, see Clay and Medwin[7]. Though more complicated expressions can be similarly derived for a given bubble size spectrum, following expressions assume an existence of a dominant bubble size of radius a.

$$F_\chi = F_{(\delta c/c_0)s} = -1 \quad \text{when } \chi=(\delta c/c_0)_s$$

$$F_\chi = F_{N0} = 2\pi a/(\omega_R/c_0)^2 \quad \text{when } \chi = N_0$$

$$F_\chi = F_{\eta 1} = 2\pi a/(\omega_R/c_0)^2 \ (g/30a_{CH})(2.9X10^6)$$

$$\text{or} \quad F_\chi = F_{\eta 2} = 2\pi a/(\omega_R/c_0)^2 \left\{g(T/\mu)/30a_{CH}\right\}(2.9X10^6)$$

$$\text{or} \quad F_\chi = F_{\eta 3} = 2\pi a/(\omega_R/c_0)^2 \ (gC_m/30a_{CH})(2.9X10^6)$$

$$\text{when } \chi = \eta_k, \ k=1,2,3$$

$$F_\chi = F_w = 29\pi a/(\omega_R/c_0)^2 \quad \text{when } \chi=W$$

$$F_\chi = F_{Mv0} = 1/\left\{2a(\omega_R/c_0)^2\right\} \quad \text{when } \chi = M_{v0}.$$

where

ω_R = resonant circular acoustic frequency

g = gravity acceleration

a_{CH} = 0.0185 = Charnock constant

T = surface tension

μ = dynamic viscosity of water

C_m = minimum surface wave velocity

This means that the volumetric scattering characteristics $d\Gamma(\underline{k})=\Gamma(\underline{k})d\underline{k}$ can be estimated not only from the direct measurement of $(\delta c/c_0)_s$ but also from the indirect measurements of N_0, η_k, W, M_{v0}. The proportional relationship between $(\delta c/c_0)$ and η_k requires the assumption of Charnock's dimensional power law[8] to be 3 which is higher than his original value of 2 and also higher than the maximum empirical value of 2.5 suggested by Wu[8]. Although there is no direct evidence that the assumption is justified at this time, it is a plausible way by which the

roughness element roughness η_k and surface roughness η can be simply correlated. Depending on the assumption of controlling physical parameters in Charnock's relationship, $F_{\eta k}$ takes different expression. $F_{\eta 1}$ results if gravity only is important (Charnock's original assumption). $F_{\eta 2}$ results if gravity, surface tension, and viscosity are all important (suggested by Wu[8]). $F_{\eta 3}$ results if gravity and surface tension are important as suggested by reference 1. In the following preliminary estimates, $F_{\eta 1}$ is utilized. The reason for using this expression as the first trial in checking experimental data is that gravity wave spectrum is the only one documented at this time.

The simple depth-wise exponential decay in equation (2-1) was confirmed by measurements of different physical quantities. Thorpe[9] had shown also that the functional form is a solution to a vertical diffusion equation. The spatial coordinates dependence of $(\delta c/c_0)$ in a product form of equation (2-1) implies also the following product form:

$$\Gamma(\underline{k}) = \Gamma(\underline{k}_{2D}, k_z) = \Gamma_z(k_z)\ \Gamma_\chi(\underline{k}_{2D}) \tag{2-2}$$

where

$$2\pi\Gamma_z(k_z) = -2k^2 \int \exp(ik_z\ z_0 - \beta z_0) F_\chi(z_0) dz_0 \tag{2-3}$$

$$(2\pi)^2 \Gamma_\chi(\underline{k}_{2D}) = \int \exp(i\underline{k}_{2D}\underline{x}_{2D}) \chi(\underline{x}_{2D}) d\underline{x}_{2D} \tag{2-4}$$

The extent of F_χ dependence on depth depends on a selected physical variable for χ. One interesting observation made by Wu[10] was the fact that the bubble size spectra of two experiments were found to be approximately invariant with either the depth or the wind velocity. Therefore depth dependence of a is probably negligible. There is a small depth dependence for ω_R. In the following estimates, however, the value of F_χ will be assumed a depth averaged constant. Thus, integration in equation (2-3) can be easily performed. Γ_z and F_χ are considered determinestic while Γ_χ and χ are considered random.

Now, the reflected field velocity potential $\phi_r(\underline{x}_{2D},z,t)$ can be re-written in terms of random variables $d\Gamma_\chi$ and dA. An appropriate statistical average is the cross-correlation

$$\langle \phi_r(\underline{x}_{2D},o,t)\ \phi_r^*(\underline{x}_{2D}+\underline{\xi},o,t)\rangle$$

where $\langle\ \rangle$ represents an ensemble average while $\underline{\xi}$ represents a horizontal separation. The reflected field spectrum $\Pi(\underline{k}_{r,2D})$ is then given by the Fourier integral

$$\Pi(\underline{k}_{r,2D}) = (1/2\pi)^2 \int \exp(i\underline{k}_{r,2D}\cdot\underline{\xi})\ \langle \phi_r(\underline{x}_{2D},0)\phi_r^*(\underline{x}_{2D}+\underline{\xi},0)\rangle d\underline{\xi}.$$

The result is given below.

$$\Pi(k_{r,2D}) = [\text{Specular Terms}]\ \delta(\underline{k}_{i,2D} - \underline{k}_{r,2D})$$

$$+(1/4)\{2\pi\Gamma_{zI}(k_z=k_{rz})/k_{rz}\}\{2\pi\Gamma_{zI}^{*}(k_z'=k_{rz})/k_{rz}^{*}\}\Phi_{\chi\chi}(\underline{k}_{i,2D}-\underline{k}_{r,2D})$$

$$+ 4\,k_{iz}^{2}\Phi_{AA}(\underline{k}_{i,2D}-\underline{k}_{r,2D})$$

$$+ k_{iz}[2\pi\Gamma_{zI}^{*}(k_z=k_{rz})/k_{rz}+2\pi\Gamma_{zI}(k_z=k_{rz})/k_{rz}^{*}]\Phi_{\chi A}(\underline{k}_{i,2D}-\underline{k}_{r,2D})$$

(2-5)

where $\underline{k}_r = (\underline{k}_{r,2D}, k_{rz})$, $\underline{k}_i = (\underline{k}_{i,2D}, k_{iz})$, $\underline{k} = (\underline{k}_{2D}, k_z)$, $\Gamma_{zI}(k_z) = -\Gamma_z(-k_{iz}-k_z) + \Gamma_z(-k_{iz}+k_z) + \Gamma_z(k_{iz}-k_z) - \Gamma_z(k_{iz}+k_z)$, and specular terms = 1- energy loss due to scattering in all directions. Spectra Φ_{AA}, $\Phi_{\chi\chi}$, and $\Phi_{\chi A} = \Phi_{A\chi}$ for roughness (η) correlation, χ correlation, and χ-η cross-correlation, respectively are defined below.

$$\langle\eta(\underline{x}_{2D})\eta^{*}(\underline{x}_{2D}+\underline{r}_{2D})\rangle = \int\exp(i\underline{k}_{2D}\cdot\underline{r}_{2D})\Phi_{AA}(\underline{k}_{2D})d\underline{k}_{2D}$$

$$\langle\chi(\underline{x}_{2D})\chi^{*}(\underline{x}_{2D}+\underline{r}_{2D})\rangle = \int\exp(i\underline{k}_{2D}\cdot\underline{r}_{2D})\Phi_{\chi\chi}(\underline{k}_{2D})d\underline{k}_{2D}$$

$$\langle\chi(\underline{x}_{2D})\eta^{*}(\underline{x}_{2D}+\underline{r}_{2D})\rangle = \langle\eta(\underline{x}_{2D})\chi^{*}(\underline{x}_{2D}+\underline{r}_{2D})\rangle$$

$$= \int\exp(i\underline{k}_{2D}\cdot\underline{r}_{2D})\Phi_{\chi A}(\underline{k}_{2D})d\underline{k}_{2D}$$

$$= \int\exp(i\underline{k}_{2D}\cdot\underline{r}_{2D})\Phi_{A\chi}(\underline{k}_{2D})d\underline{k}_{2D}$$

The reflected field spectrum above exhibits the same features as those of ocean surface roughness scattering[11], ocean bottom roughness scattering[3,12], and under-ice roughness scattering[13]. The reflected field spectrum has two components. The specular component contains a factor of Dirac Delta function which indicates a concentrated energy in the specular direction. The specular component depends on the entire wave number domain of spectrum associated with the scattering physical quantities such as surface roughness, fluctuating sound velocity, etc. The rest is the off-specular component which depends only on a particular (selected) wave number defined by the incident wave and a selected (reflected) wave number. The specular component can be utilized to estimate (forward) reflection loss which will be reported in the future. The off-specular component can-be utilized to estimate scattering strength. The back-scattering strength in particular is addressed here. The usual scattering strength m" is given by $k^2\nu_r^2\Pi(\underline{k}_{r,2D})$ where ν_r is the direction cosine of a reflected wave with respect to the vertical axis. Accordingly m" written in terms of direction cosines ($k_{iz} = k\gamma$, $k_{rz} = k\nu_r$) is given by the following expression. (γ,ν_r) are direction cosines of (incident, reflected) waves with respect to the vertical axis.

$$m" = 4\, k^4\gamma^2\nu_r^2[\Phi_{AA}(\underline{k}_{i,2D}-\underline{k}_{r,2D}) - 2\{4\beta F_\chi k^2/[(k^2(\gamma+\nu_r)^2+\beta^2)\cdot$$

$$\cdot(k^2(\gamma-\nu_r)^2+\beta^2)]\}\Phi_{\chi A}(\underline{k}_{i,2D} - \underline{k}_{r,2D})+\{4\beta F_\chi k^2/[(k^2(\gamma+\nu_r)^2+\beta^2)\cdot$$

$$\cdot(k^2(\gamma-v_r)^2+\beta^2)]\}^2\Phi_{\chi\chi}(\underline{k}_{i,2D}-\underline{k}_{r,2D})]$$

(2-6)

The back-scattering strength m_B'' ($10\log_{10} m_B''$ in dB level) is thus obtained by setting $\underline{k}_{r,2D} = -\underline{k}_{i,2D}$ (also $\gamma = v_r$) in the above equation. It results in the following expression:

$$m_B'' = 4k^4\gamma^4[\Phi_{AA}(2\underline{k}_{i,2D})-2\{4\beta F_\chi k^2/[(4k^2\gamma^2+\beta^2)\beta^2]\}\Phi_{\chi A}(2\underline{k}_{i,2D})$$

$$+\{4\beta F_\chi k^2/[(4k^2\gamma^2+\beta^2)\beta^2]\}^2\Phi_{\chi\chi}(2\underline{k}_{i,2D})].$$

(2-7)

In order to estimate backscattering strength, spectra ($\Phi_{AA}, \Phi_{\chi A}, \Phi_{\chi\chi}$), and β should be estimated first. An example is worked out in the next section for demonstrating its use.

3. An Example and its Physical Implications

The following predictions are based on plausible assumptions of $\chi = \eta_1 = \eta$ and $\Phi_{\chi A} = \Phi_{A\chi} = 0$. Physically, the wave breaking roughness elements are assumed in the first assumption to serve also as surface roughnesses that scattered sound. In the second assumption, η and η_1 are assumed not correlated. This may be partly justified by the fact that plume penetration takes time and the local volume scattering bubbles may not have been generated by the local breaking roughnesses. Then equation (2-7) is given by:

$$m_B'' = 4\, k^4 \gamma^4 [1+\{4\beta F_\chi k^2/[(4k^2\gamma^2+\beta^2)\beta^2]\}^2]\Phi_{AA}(2\underline{k}_{i,2D}) \tag{3-1}$$

where

$$F_\chi = F_{\eta 1} = 2\pi a/(\omega_R/c_0)^2 (g/30a_{CH})(2.9 \times 10^6)$$

$$= 2\pi a(10^{-6})/\left(\frac{2\pi}{c_0}\,\frac{3.25\times10^6}{a}\,\sqrt{1+0.1z}\right)^2 \cdot (9.8/30\times0.0185)\,(2.9\times10^6)$$

$$\simeq 1.616 \times 10^{-6}\, a^3$$

a = bubble radius in μm

$1 + .1z$ = 1.075 average over 1.5 m depth

β = $1/l_z$ (1/m)

k = 0.0041867f (1/m)

$|2\underline{k}_{i,2D}| = 2k\sqrt{1-\gamma 2} = 0.0083734\ f\ \cos\theta_g$

θ_g = grazing angle

$\Phi_{AA}(k_B) = 8.1X10^{-3}/(4\pi k_B^4)\ \exp\ [-0.74g^2/U^4k_B^2]$

= Pierson - Moskowitz[14] Spectrum

$\gamma = \cos\theta_i = \sin\theta_g$

θ_i = incident angle.

Substitution of above numerical numbers into equation (3-1) results in the following equation:

$$m_B'' = [1+\{1.133 \times 10^{-10} f^2 (al_z)^3/(1+7.01x10^{-5} f^2 \sin\theta_g l_z^2)\}^2] \cdot$$

$$\cdot 1.61x10^{-4} \tan^4\theta_g \exp\ [-1.01x10^6/f^2\cos^2\theta_g U^4)]$$

= [1 + Volumetric Factor] (Surface Scattering Effect)

(3-2)

Accordingly, the back-scattering strength has two independent components. One component estimates the surface scattering effect and has the exact form utilized by Ogden/Erskine[15]. The other component estimates the volumetric scattering effect and is given in this example in terms of the surface scattering effect multiplied by a volumetric factor. This volumetric factor is the sum of the product of plume penetration effect and F_χ as originally given in the form of equation (2-3) and specifically for this example it results in equation (3-1). The parameter

$l_z=(1/\beta)$ quantifies the extent of plume penetration. The parameter "a" stress the bubble size dependence on relating $(\delta c/c_0)$ to other physical parameters. There is an indication that l_z depends on the wind speed. The dependence of bubble size on wind speed is less known. For instance, the bubble size spectrum was concluded by Wu[10] to be approximately invariant with either the depth or wind speed.

Before numerical computation, it will be helpful (1) to review the validity of (2) to investigate the qualitative behavior of equation (3-2).

Major assumptions made were the applicability of perturbation method for both volumetric and surface scattering. For volumetric scattering, it amounts to assuming the validity of single volumetric scattering. It has been estimated[1] that the assumption requires acoustic frequencies to be not higher than 1000 Hz. For surface scattering, the perturbation approximation requires maximum wind speed to be limited to about 13 knot and 30 knot for 1000 Hz and 100 Hz, respectively. Therefore, the following predictions for frequencies 200 Hz and lower are more reliable at high wind speeds. Though the following predictions are better than those of previous investigators, McDonald[5] and Henyey[6], who did not include surface scattering effect and utilized far-field approximation, predictions at high frequencies around 1000 Hz for wind speeds exceeding 13 knot are considered preliminary. In the future, it may be somewhat generalized by the composite-roughness scattering concept (see e.g. McDaniel et al[16], Jackson et al[17]). Fortunately, where the surface

scattering perturbation is questionable, the volumetric scattering dominates and volumetric perturbation is valid.

The qualitative behavior of equation (3-2), depends critically on the magnitude of the volumetric factor. It can be easily seen that the volumetric factor is much less than one for small values of (f, l_z, a) where $k = 2\pi f$. This means that the back-scattering strength is dominated by the surface scattering phenomena when frequency or wind speed is low. This qualitative prediction is consistent with the experimental data summary presented by Ogden/Erskine[15]. It can also be shown that the volumetric scattering effect dominates when l_z or wind speed is sufficiently high. There is an interesting coincident observation. In summarizing the experimental data on characteristic depth, l_z here, Wu[10] concluded that l_z stayed at a low constant value of about 0.4m up to about 14 knot wind speed and then suddenly increased linearly with wind speed to a l_z value of about 1m at 23 knot. Ogden/Erskine[15] also concluded that the back-scattering strength increased suddenly beyond this critical wind speed for higher frequency acoustic waves - the increase was presumed to be caused by the volumetric scattering effect. These two observations can be linked together by equation (3-2). Equation (3-2) also predicts less increase in the volumetric scattering effect for a higher grazing angle. This prediction is also consistent with the back-scattering data by comparing data for 10° and 30° grazing angles. Quantitative predictions follow.

Special phenomena of interest are (1) the critical wind speed

beyond which the volumetric scattering dominates and (2) the excess dB level due to the volumetric scattering. Following estimates assume a=60 μm.

At critical wind speed, the volumetric factor becomes an order of one. For a given frequency and a grazing angle, a critical l_z can be obtained. Then the critical wind speed can be obtained from the expression describing l_z dependence on wind speed. In general, l_z (in m) increases with wind speed (U in ms^{-1}). Wu[10] proposed the following two relationships.

$$l_z = 0.4m \qquad \text{when } U<7ms^{-1}(=14 \text{ knot})$$

$$l_z = 0.4+0.12(U-7)m \qquad \text{when } U>7ms^{-1} \tag{3-3}$$

and

$$l_z = 0.85 \qquad \text{when } U<7ms^{-1}$$

$$l_z = 0.85+0.12(U-7)m \qquad \text{when } U>7ms^{-1} \tag{3-4}$$

Equation (3-3) is based on the bubble population data of Kolovayev[18], Johnson and Cooke[19] and on the acoustic cross section data of Thorpe[20]. Equation (3-4) is based on the acoustic cross section data of Crawford and Farmer[21]. The wind independency of l_z up to $7ms^{-1}$ wind velocity is a curious

physical phenomenon that should be investigated further in the future. Up to now, the temptation is to exclusively conjecture the phenomenon as being due to biological activities. There may be other explanations that are dynamic in nature. The estimated critical wind speeds for different frequencies and grazing angles are tabulated in Table 1 and depicted in Figure 2 and Figure 3.

The excess dB level due to the volumetric scattering is estimated by 10 $\log_{10}$ [1+(volumetric factor)] and added to the surface scattering level 10 $\log_{10}$ [surface scattering effect] to obtain the total backscattering level. The predicted excess dB levels are tabulated in Table 1. The predicted total backscattering levels are depicted in figures 2 through 5.

For 50Hz and either 10° or 30° grazing angle, the estimated critical wind speeds utilizing either equation (3-3), denoted by Wu, or equation (3-4), denoted by C/F, are higher than 30 knots. This means that the surface scattering effect dominates and the excess dB level due to the volumetric scattering is negligible (zero in Table 1) even beyond wind speed of 30 knots. These predictions are consistent with data summary of Ogden and Erskine[15] (O/E) as shown in Figure 2 and Figure 3 in which no critical wind speed was observed for 50 Hz case up to wind speed of 30 knot. The 50 Hz total backscattering levels at 30 knot wind speed were estimated and depicted on Figure 5. Since the backscattering levels are dominated by the surface scattering effect, the term that requires the use of either Equation (3-3) or Equation (3-4) is negligible and the estimated levels are both identical to those of Ogden and Erskine shown in Figure 5. The

same conclusion can be made on the 100 Hz backscattering levels for a given wind speed of 5 knot as shown in Figure 4.

For 200 Hz and either 10° or 30° grazing angle, the estimated critical wind speeds and backscattering levels are closer to O/E data, if equation (3-4) or C/F is utilized as in Table 1, Figure 2, and Figure 3. The results stress the importance of l_z effect on both critical wind speeds and the backscattering levels. Though the comparison of predictions and experimental data for 30° grazing angle case is not as good as that of 10° case, the trend of lower excess dB due to volumetric scattering is successfully predicted.

The importance of l_z effect on backscattering is further demonstrated by the case of 1000 Hz. The use of lower l_z values given by Wu, predicted a critical wind speed of O/E for 10° grazing angle (Figure 1) but much higher value for 30° grazing angle (Figure 3). The predicted excess dB levels above these critical wind speeds are lower than those observed by O/E in general. However, the use of higher l_z values given by C/F predicted no critical wind speed for either 10° or 30° grazing angle case - i.e. the volumetric scattering dominance is predicted at wind speed as low as 6 knots. In Figure 2, the data of Christian and Tattersall[22] (C/T), Chapman and Harris[23]/Chapman and Scott[24] (CH/CS), and Chester[25] (CST7) are presented. Though these data are for 7° grazing angle, they clearly indicate no critical wind speed above 6 knots. The trend is similar to that predicted by utilizing higher l_z values of C/F. If l_z data of C/F are indeed mixed with bubble population of biological

activities (beside wind wave generated) as speculated by Wu[10], then the wave mixing tends to produce more scattered l_z data as indicated by the original data of Crawford and Farmer[21]. This implies that the spread of backscattering levels in the region of Figure 2 between those predicted by C/F(1000) and Wu(1000) is quite possible. As expected, the predicted grazing angle dependence at low wind speed for 1000 Hz (Figure 4) compares quite well with that of O/E data if lower l_z values of Wu are used (when C/F l_z values are used, levels are closer to C/T data). At high wind speed of 30 knots (Figure 5), the predicted grazing angle dependence compares well with O/E data only at low grazing angles and if higher l_z data of C/F is utilized.

4. Conclusions and Recommendations

The preliminary analysis based on selecting roughness element height as a choice physical parameter, succeeded in predicting observed features of backscattering strength levels, such as a critical wind speed beyond which volumetric scattering dominated. It was especially interesting that this critical wind speed corresponded to the wind speed beyond which l_z suddenly increased linearly with the wind speed. It was also found that wind speeds alone could not uniquely define l_z and that quite different backscattering strength levels were predicted for different experimental data set taken at the same apparent wind speed. If wind speed were to be used, one should use additional parameters such as wind fetches and durations. Otherwise one may use local physical parameters such as wave heights or friction velocities suggested by Wu[8].

Similar analyses based on choices of other physical parameters should be performed to relate scattering strength with those parameters, e.g. N_0, W, and M_{v0}. These analyses require information on their cross-correlations or their wave number spectra of these chosen physical parameters. It will be better if those physical parameters are measured simultaneously with backscattering data. CST-7 was such an experiment and its data should be utilized. Then the prediction of reflection loss should be performed. If successful, the same mathematical method can be utilized to evaluate ocean bottom scattering when volumetric scattering is important.

References

1. E.Y.T. Kuo, "The Perturbation Characterization of Reverberations From A Wind Generated Bubbly Ocean Surface - I. Theory And Scattering Strength Predictions", under preparation, 1992.

2. E.Y.T. Kuo, "The Perturbation Characterization of Ocean Reverberations", NATO Ocean Reverberation Symposium, La Spezia, Italy, 25-29 May 1992.

3. E.Y.T. Kuo, "Wave scattering and transmission at irregular surfaces," J. Acoust. Soc. Amer., vol. 36, pp. 2135-2142, 1964.

4. G.K. Batchelor, "Wave scattering due to turbulence," Symposium on Naval Hydrodynamics, Washington, D.C., 1956.

5. B.E. McDonald, "Echoes from vertically stratified subresonant bubble clouds: a model for ocean surface reverberation," J. Acoust. Soc. Amer., vol. 89, pp. 617-619, 1991.

6. F.S. Henyey, "Acoustic scattering from ocean microbubble plumes in the 100 Hz to 2 kHz region," J. Acoust. Soc. Amer., vol. 90, pp. 399-405, 1991.

7. C.S. Clay and H. Medwin, Acoustical Oceanography: Principles and Applications. New York: John Wiley & Sons, 1977.

8. J. Wu, "Wind-stress coefficients over sea surface near neutral condition - a revisit," J. Physical Oceanography, vol. 10, pp. 727-740, 1980.

9. S.A. Thorpe, "On the determination of Kv in the near surface ocean from acoustic measurements of bubbles," J. Physical Oceanography," vol. 14, pp. 855-863, 1984.

10. J. Wu, "Individual characteristics of whitecaps and volumetric description of bubbles," IEEE J. Oceanic Engineering, vol. 17, pp. 150-158, 1992.

11. E.Y.T. Kuo, "Sea surface scattering and propagation loss: review, update, and new predictions," Invited Paper, IEEE J. Oceanic Engineering, vol. 13, pp. 229-234, 1988.

12. E.Y.T. Kuo, "Acoustic wave scattering from two solid boundaries at the ocean bottom: reflection loss," IEEE J. Oceanic Engineering, vol. 17, pp. 159-170, 1992.

13. E.Y.T. Kuo, "Low Frequency Acoustic Wave Scattering Phenomena, Under Ice Cover," J. Oceanic Eng./IEEE, 15, 361-372(1990).

14. W.J. Pierson, Jr. and L. Maskowitz, "A Proposed Spectral Form for Fully Developed Wind Seas Based on the Similarity Theory of S.A. Kitaigorodskii," J. Geophy. Res., 69, pp. 5181-5190, 1964.

15. P.M. Ogden and F.T. Erskine, "An Empirical Prediction Algorithm for Low Frequency Acoustic Surface Scattering Strengths," NRL/FR/5160-92-9377, Naval Research Laboratory, Washington, D.C., 1992.

16. S.T. McDaniel and A.D. Gorman, "An Examination of the Composite-Roughness Scattering Model," J. Acoust. Soc. Am., 73, pp. 1476-1486, 1983.

17. D.R. Jackson, D.P. Winebrenner, and A. Ishinaru, "Application of the composite roughness model to high-frequency bottom backscattering," J. Acoust. Soc. Am., 79, pp. 1410-1422, 1986.

18. P.A. Kolovayev, "Investigation of the concentration and statistical size layer distribution of wind-produced bubbles in the near-surface ocean," Oceanology, 15, pp. 659-661, 1976.

19. B.D. Johnson and R.C. Cooke, "Bubble population and spectra in coastal water: A photographic approach," J. Geophys. Res., 84, pp. 3761-3766. 1979.

20. S.A. Thorpe, "On the clouds of bubbles formed by breaking wind-waves in deep water and their role in air-sea gas transfer," Phil. Trans. Roy. Soc. Lond., A304, pp. 155-210, 1982.

21. G.B. Crawford and D.M. Farmer, "On the spatial distribution of ocean bubbles," J. Geophy. Res., 92, pp. 8231-8243, 1987.

22. R.J. Christian and J.M. Tattersall, "Amplitude and Spectral Characteristics of Convergence Zone Surface Reverberation," NUWC TR#9013, Naval Undersea Warfare Center, New London Detachment, New London, CT, 1991.

23. R.P. Chapman and J.H. Harris, "Surface Backscattering Strengths Measured with Explosive Sound Sources," J. Acoust. Soc. Am., 34, 1592-1597, October 1962.

24. R.P. Chapman and H.D. Scott, "Surface Backscattering Strengths Measured Over an Extended Range of Frequencies and Grazing Angles," J. Acoust. Soc. Am., 36, 1735-1737(L), 1964.

25. J.B. Chester, "Low-Frequency Single Interaction Acoustic Scatter From the Sea Surface Using Short Pulses," Paper 5PUWZ, 124th ASA Meeting, 1992.

FRE(HZ)			50		200		1000		NOTE
G. ANGLE(°)			10°	30°	10°	30°	10°	30°	
CRITICAL		CRITICAL l_z(m)	2.56	2.8	1,035	1.31	.375	.782	
CRITICAL	UNKNOT	Wu	48	52	24	28	14	20	
		C/F	41	45	17	21	<6	≤6	Wu's interpretation
		O/E	>30	>30	18	18	14	14	
		C/T	-	-	-	-	<6	-	7° Grazing Angle
VOL. EXCESS DB	6 UNKNOT	Wu	0	0	0	0	0	.7	
		C/F	0	0	0	0	15.6	3.4	Wu's interpretation
		O/E	0	0	0	0	0	0	
		C/T	-	-	-	-	10	-	7° Grazing Angle
	30 UNKNOT	Wu	0	0	8.2	3.6	22.5	6.7	
		C/F	0	0	14	6.4	25.6	8.8	Wu's interpretation
		O/E	0	0	20	11	30	20	
		C/T	-	-	-	-	20	-	7° Grazing Angle

TABLE 1 Backscattering Phenomena and e-folding bubble Plume Depth (l_z):

Wu = (Kolovayev, Johnson/Cooke, Thorpe)

C/F = Crawford/Farmer, O/E = Ogden/Erskine,

C/T = Christian/Tattersall

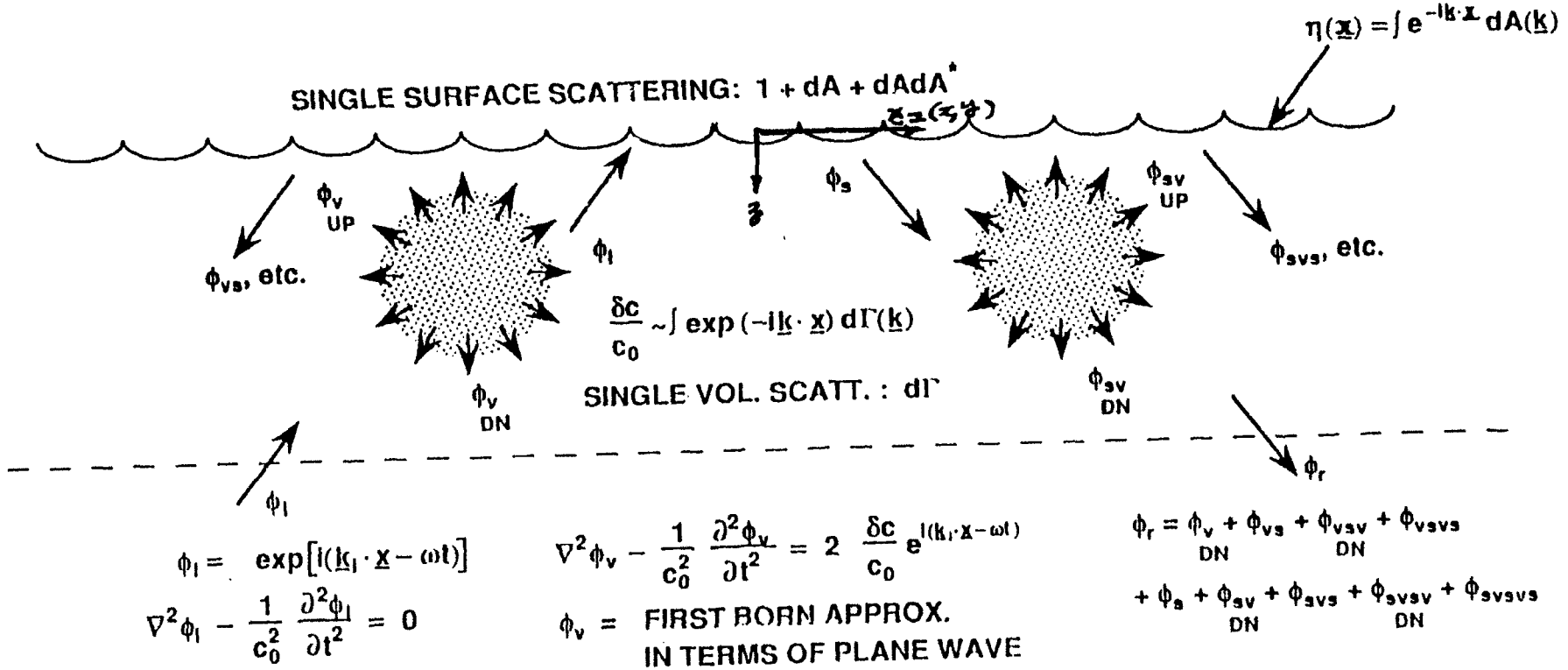

Fig. 1. The model

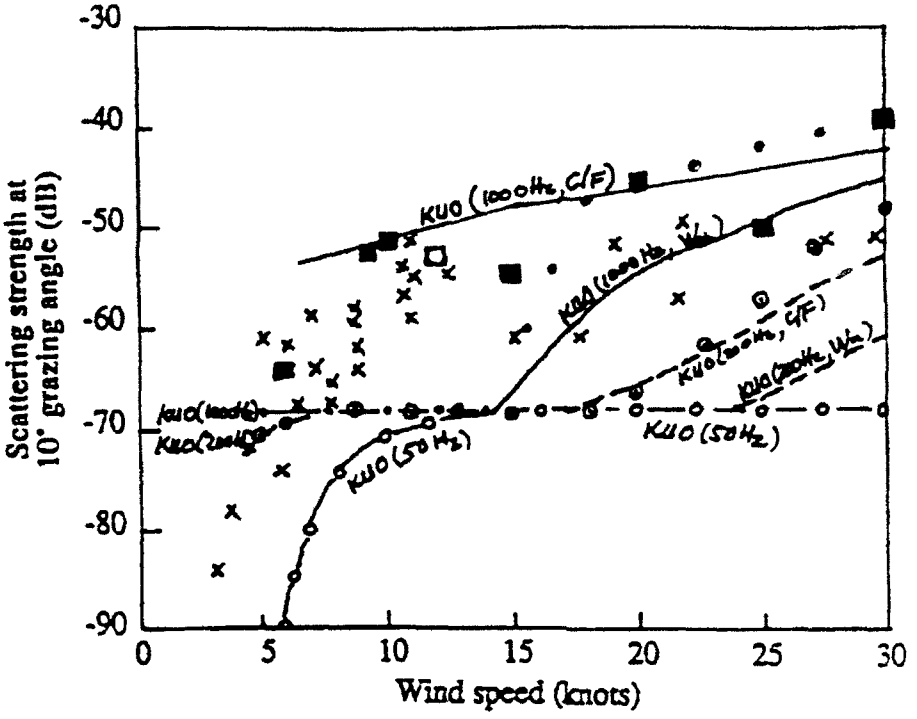

Fig.2 – Back - scattering strengths as a function of wind speed and frequency for a grazing angle of 10°

• • • O/E (1000 Hz, 10°)
⊙ ⊙ ⊙ O/E (200 Hz, 10°)
∘ ∘ ∘ O/E (50Hz, 10°)
× × × C/T (1000Hz, 7°)
■ ■ ■ CH/CS (1000Hz, 7°)
□ CST-7 (1000Hz, 7°)

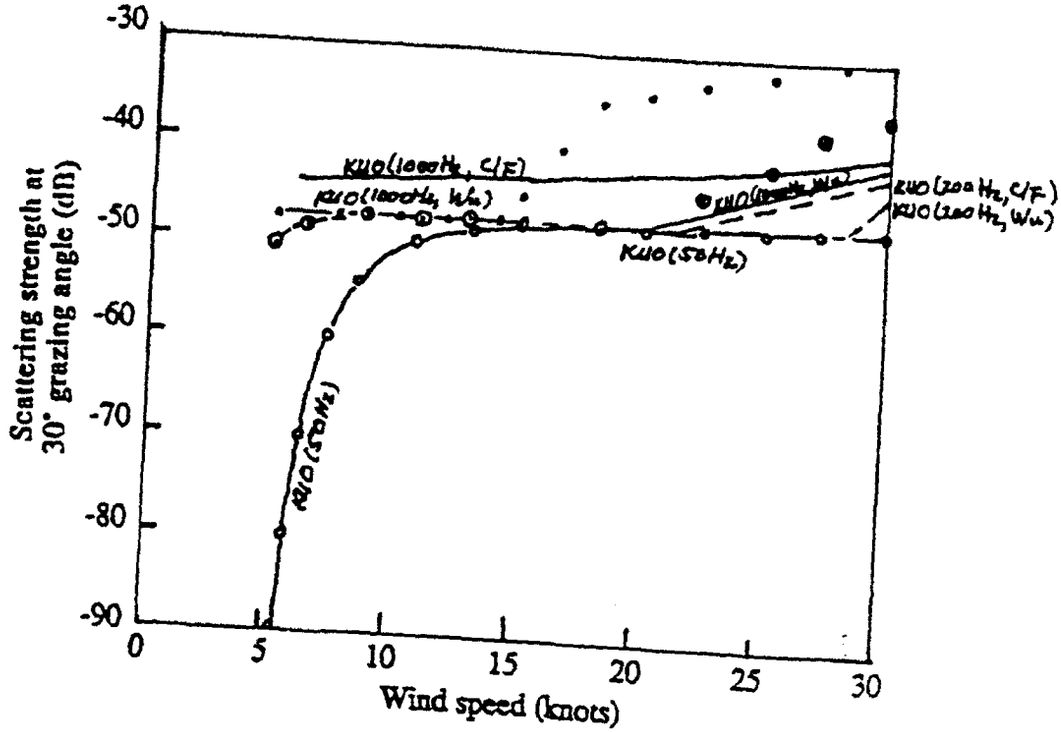

Fig. 3 - Back scattering strengths as a function of wind speed and frequency for a grazing angle of 30°

• • • σ/E (1000Hz)
◎ ◎ ◎ σ/E (200Hz)
o o o σ/E (50Hz)

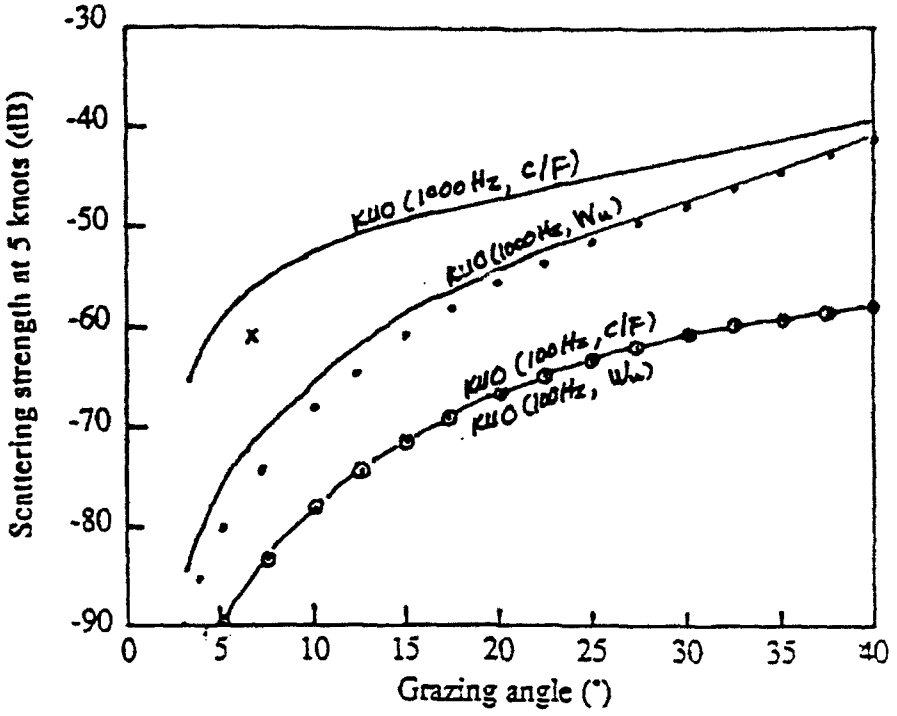

Fig. 4 – Best scattering strengths as a function of grazing angle and frequency for a wind speed of 5 knots

x C/T (1000 Hz, 7°)

• O/E (1000 Hz)

⊙ O/E (100 Hz)

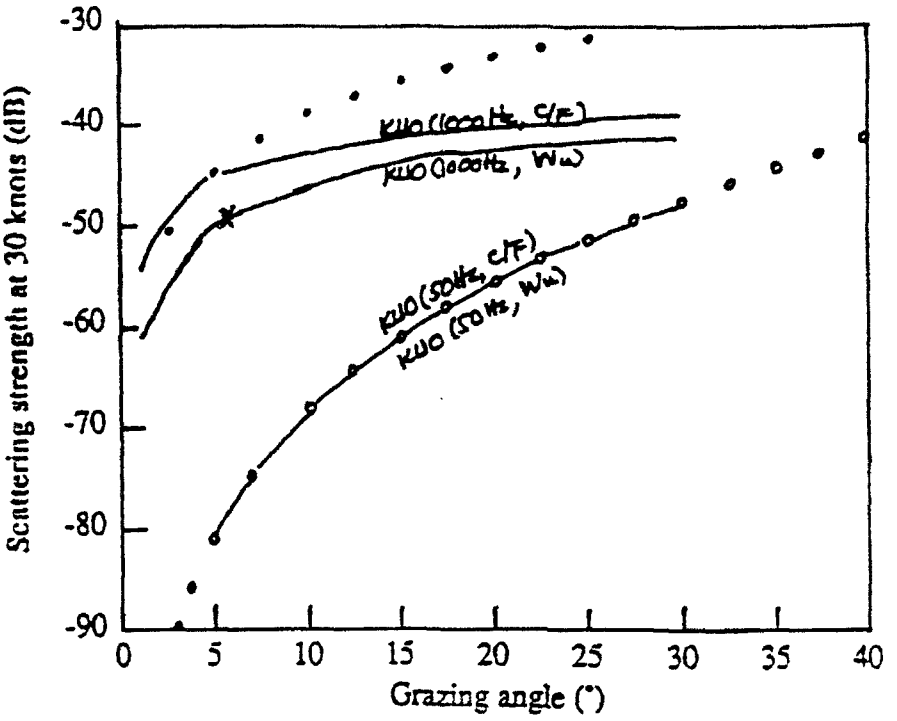

Fig. 5 – Back scattering strengths as a function of grazing angle and frequency for a wind speed of 30 knots

- • O/E (1000 Hz)
- o O/E (50 Hz)
- x C/T (1000 Hz, 7°)

INITIAL DISTRIBUTION LIST

Addressee	No. of copies
NAVSEA [PEO USW ASTO, D. Spires]	1
Johns Hopkins University/APL [B. Newhall, J. Sweeney, A. Boyles, J. Hanson, S. Hazek]	5
NRL [B. Palmer, F. Erskine, R. Gauss, P. Ogden, R. Pitre, E. McDonald, J. Berkson, D. Wurmser R. Gragg, Library]	10
NRL/SSC [E. Franchi, J. Matthews, R. Love, J. Caruthers, R. Field, Library]	6
CNO [R. Winokur (NOP 96T)]	1
ONR [R. Feden, K. Dial, E. Chaika, E. Estallotte, G. Kovalenko]	5
ARL/UT [J. Shooter, S. Mitchell, Library]	3
SAIC/McLean [R. Dicus, A. Eller, C. Spofford, L. Dozier, R. Cavanaugh]	5
SAIC/New London [F. DiNapoli]	1
BBN/New London [P. Cable, J. Bairstow]	2
BBN/Cambridge, MA [G. Shepard, D. Bosek, M. Frey, J. Heine]	4
BBN/Arlington [T. Kooij]	1
DARPA/MSTO [W. Carey]	1
ARL/PSU [D. McCammon]	1
APL/UW [C. Sienkiewicz, E. Thorsos, D. Jackson, F. Henyey, L. Crum, P. Dahl, Myamoto]	7
Kildare Corp. [R. Mellem]	1
Defense Research Establishment Pacific [D. Thomson, R.P. Chapman]	2
Defense Research Establishment Atlantic [B.Franklin]	1
FWG [P. Willie, H. Baur, H. Herwig, B. Nutzel, Bibliotek]	5
DTIC	12
SACLANTCTR [Technical Director, O. Diachok, Library (2)]	4
NAVPGSCOL [Library, H. Medwin]	2
Arete [M. Huster, S. McConnell]	2
AT&T [R.L. Holford]	1
Tracor/New London [G. Heines, S. Reilly]	2
SPAWAR PMW182 [C. Bohman]	1

INTERNAL DISTRIBUTION

NEW LONDON

Code	
01Y	J. Kyle
0261	Library (2)
10	W. Roderick
211	T. Fries
212	
2122	
30	D. Counsellor
304	C. Mason, D. Ashworth
31	B. Cole
311	R. Radlinski
3112	R. Christian, J. Chester (3), D. Chizhik, R. Deavenport, L. Dillman, R. Nielsen, R. Saenger, M. Sundvik, J. Tattersall, M. Vaccaro
3111	D. Klingbeil, S. Capizzano, J. Turner, T. Baus
312	M. Gerber
3121	R. Dullea, N. Fisch, W. Powers, D. Browning, M. Rosario
3122	E. Jensen, J. Bishop, H. Weinberg
313	
33	C. Nawrocki
33A	P. Herstein, A. Goodman, P. Koenigs, J. Monti, R. Malone, L. Petitpas
3314	R. Barton, R. Tremblay
332	M. Ricciuti
3321	P. Seaman, E. Kuo (5)
61	C. Batta, D. Williams

NEWPORT

Code	
0262	Library
10	K. Lima
8212	G. Bishop

External:	86
Internal:	59
Total:	145